J Appl Electrochem (2013) 43:975–984
DOI 10.1007/s10800-013-0595-5

RESEARCH ARTICLE

Application of graphene oxide sheets incorporated in the porous calcium alginate films on the glassy carbon electrode for biosensor construction based on myoglobin

Qianqian Ma · Hong Sun · Shifeng Hou

Received: 27 March 2013 / Accepted: 16 July 2013 / Published online: 26 July 2013

Abstract In this work, graphene oxide (GO) sheets were assembled within the porous calcium alginate (CA) films, and applied to fabricate electroactive biosensor by incorporating with myoglobin (Mb). The porous Mb–GO–CA films were fabricated and characterized by scanning electron microscopy (SEM), UV–Vis adsorption, and electrochemistry techniques. UV–Vis spectrum demonstrated that Mb retained its secondary structure in the porous Mb–GO–CA films at medium pH. Cyclic voltammetry of the porous Mb–GO–CA films showed a pair of well-defined and nearly reversible peaks for MbFe(III)/Fe(II) redox couple at −0.350 V versus saturated calomel electrode in pH 7.0 buffers. The electrochemical parameters such as apparent heterogeneous electron transfer rate constant (k_s) and formal potential ($E^{o\prime}$) were estimated by fitting the data of square-wave voltammetry with nonlinear regression analysis. The porous Mb–GO–CA films exhibited excellent electrocatalytic reduction to sodium nitrite, oxygen, and hydrogen peroxide, and showed good reproducibility and stability, which may provide a promising platform for the fabrication of the third-generation biosensor.

Keywords Graphene oxide sheets · Porous calcium alginate films · Myoglobin · Electrochemistry · Electrocatalysis

Q. Ma · H. Sun (✉)
Institute of Multifunctional Materials (IMM), Laboratory of New Fiber Materials and Modern Textile, College of Chemistry, Chemical Engineering and Environment, Qingdao University, Qingdao 266071, China
e-mail: sun_hong@qdu.edu.cn

S. Hou
Department of Chemistry and Biochemistry, Montclair State University, Montclair, NJ 07043, USA

1 Introduction

Graphene and its derivatives have attracted much research attention as novel material since 2004, and emerge as an interesting material in a myriad of applications because of its excellent electrical conductivity, mechanical strength, and chemical stability [1–3]. One-atom-thick and two-dimensional (2D) layers of sp^2-hybridized carbon is the basic structure of graphene. With intensive studies for many exceptional properties and applications of several other forms of sp^2-hybridized carbon including carbon nanotube and fullerene [4], it is naturally expected that graphene is prompting studies for many nanoelectronic and optoelectronic devices. The combination of the high-surface area, high conductivity, and unique graphitized basal plane structure makes graphene sheets a promising candidate for fabricated graphene-modified electrodes to study electrochemical and catalytic behavior of some biomolecules [5, 6]. Most of the graphene studies have focused on its physical properties, such as its electronic properties, and these studies have demonstrated some applications in gas sensors [7] and pH sensors [8]. A number of graphene-based sensors and biosensors have been successfully developed in electroanalytical chemistry or electrochemistry. For instance, the modified electrode based on graphene and chitosan composite film has been fabricated for immobilizing the hemoglobin [9]. It was also reported that graphene-modified electrodes could be used for determination of dopamine (DA), dihydronicotinamide adenine dinucleotide (NADH), ethanol, Cd^{2+}, Pb^{2+}, and glucose [10–13]. However, many of the interesting and unique properties of graphene can only be realized after it is integrated into more complex assemblies [14, 15]. A useful technique to incorporate graphene into such assemblies is through chemical functionalization of the

graphene, which enables chemical covalent bonding between the graphene and the material of interest. Casero et al. [16] reported that the synthesis and characterization of different kinds of graphene nanomaterials and their applicability to the development of biosensing platforms, such as graphene oxide (GO) and the electrochemically reduced graphene (ERG). Lactate oxidase was taken as a model to ascertain the key role of the GO and ERG in the electrocatalytic response of the resulting biosensor toward lactate. Experimental data showed that although the incorporation of GO or ERG to the device results in an enhancement of the analytical response of the biosensor, the former system offers slightly better analytical properties and a more reproducible response than ERG one.

GO sheets are chemically exfoliated graphite oxide sheets with hydroxyl, carboxylic groups, and epoxy groups at the edges and on the basal planes [17]. Such functional groups may play a significant role in preparing graphene-based biosensors. First, these GO sheets are more dispersible and biocompatible than other carbon-based materials due to their functional groups. And second, due to their planar morphology and thus larger accessible surface area, GO sheets may perform better than any other carbon-based-modified electrode as a biosensor. In addition, it also demonstrates its potential low-manufacturing cost as compared to other nanostructured carbon materials, such as carbon nanotubes. These advantages of GO sheets make them an ideal material for sensors. Recently, GO and GO composite materials have been used to fabricate pH sensor [18], photovoltaic device [19], supercapacitor [20], and biosensors [21]. Several studies have reported construction of electrochemical biosensors using GO [22, 23]. GO films modified on the electrode surface have been used for the study of proteins [24].

Myoglobin (Mb) was chosen as a model enzyme in this study. In this respect, it is an ideal model for the study of electron transfer reactions of heme proteins because of its commercial availability, moderate cost, and a known and documented structure [25]. Without using any chemical mediators, it can provide a model for the study of enzyme-catalyzed reaction in biological systems and may establish a foundation for the construction of the third-generation biosensors or enzymatic bioreactions [26, 27]. However, the direct transfer exchange between Mb in solution and solid electrodes is usually very slow [28]. Many researchers used promoters in Mb solution to enhance the electron transfer. A relative new avenue to realize direct electrochemistry of proteins is to incorporate proteins into films which are cast on the surface of solid electrodes [29]. The films can be fabricated by biopolymers [30], insoluble surfactants [31], hydrogel polymers [32], and inorganic–organic composite materials [33] because these films can provide a favorable microenvironment for retaining the structure of redox proteins and promote the electron transfer between electroactive center of proteins and the electrode [34].

With regard to the different biopolymers that can be employed in the formation of films, sodium alginate (SA) is one of the most frequently used [35]. In molecular terms, SA is an anionic linear polysaccharide with 1,4-linked β-D-mannuronate (M) and α-L-guluronate (G) residues either as blocks of the same units or as a random sequence of the two sugar residues [36]. The extensive use of SA is derived from their ability to form gels in the presence of divalent cations such as calcium ions. A model has been widely accepted to describe specific and strong interactions between calcium ions and G units in SA chains, popularly known as the "egg box" model [37]. Calcium ions in the model make SA gels much tight and stable. In the electrochemical field, this complex formation has been exploited and calcium alginate (CA) gels used for biocatalyst encapsulation matrices, which can provide a good biocompatible microenvironment for redox proteins immobilized on the electrode and the immobilization procedure can be carried out under very mild conditions [38].

SA was a good film-forming material for immobilizing redox proteins on electrode surfaces for studying the direct electrochemistry of the proteins [39, 40]. SA forms stable gels at room temperature in the presence of Ca^{2+} cations, which makes the gels much tight. Polyethylene glycol (PEG) is soluble in aqueous solutions and nontoxic, which was used as porogenic agent to enlarge the holes in the gels [41, 42].

Stimulated by the works of Wu and co-workers [41, 42], we used the method to create the porous CA films with calcium chloride solution ($CaCl_2$) as cross-linking agent and PEG as a porogenic agent for the immobilization of Mb [43]. In this new kind of porous CA–Mb film, Mb retained its native structure and displayed good direct electrochemistry and electrocatalytic properties.

The present work is our further attempt in this direction. It will be attractive to incorporate GO sheets into the porous CA films on the electrode surfaces, because such a novel porous GO–CA films may generate synergy on electrocatalytic activity and thus enhance the sensitivity of the biosensor. The main objective of this work was to evaluate the use of GO sheets incorporated in the porous CA films as a matrix for enzyme immobilization. While Mb was cast on the porous CA–GO films, the composite porous Mb–GO–CA film was formed. Some of the films' characteristics, such as the stability and diffusional properties of the films were examined. Furthermore, apparent kinetic parameters of the incorporated Mb were tested. And the direct electron transfer of Mb and electrocatalytic activity toward various substrates, such as sodium nitrite ($NaNO_2$), oxygen (O_2) and hydrogen peroxide (H_2O_2), were investigated.

2 Experiments

2.1 Chemicals

Horse heart myoglobin (Mb, M_W 17 800) was obtained from Sigma. SA, polyethylene glycol (PEG, M_W 4 000), and potassium ferricyanide ($K_3[Fe(CN)_6]$) were obtained from Tianjin Yuanhang Chemical Corporation, Shanghai Chemical Reagents Corporation, and Qingdao Chemical Engineering Plant, respectively. Other chemicals, such as H_2O_2 (30 %), $CaCl_2$ and $NaNO_2$ were of analytical grade and used without further purification.

The buffer solutions with various pH values were prepared by mixing 0.05 M sodium acetate, 0.05 M sodium dihydrogen phosphate, 0.05 M citric acid, or 0.05 M boric acid with 0.1 M potassium bromide. The pH of buffers was adjusted with HCl or NaOH solutions. Double-distilled water was used in this experiment throughout. The working solutions of $NaNO_2$ and H_2O_2 were freshly prepared before being used.

GO prepared through Hummers' method [44] was used in this study. The synthesis process started with chemical oxidation of graphite flakes, the resultant graphite oxides were then split apart by ultrasonication method to yield single but wrinkled GO sheets. Subsequently, the prepared GO sheets were filtrated and purified, which were dispersed in double-distilled water before used in experiment [45].

2.2 Apparatus and measurements

All electrochemical measurements were performed with a CHI 760C electrochemical workstation (Shanghai CH Instruments, China) in a conventional three-electrode cell at ambient temperature and GC electrode was selected as working electrode, a saturated calomel electrode (SCE) as reference electrode, and a platinum wire as counter electrode.

Buffers contained in the cell were thoroughly deoxygenated with pure nitrogen for at least 10 min prior to the experiments, and retained under nitrogen atmosphere during the experiments. Reduction of oxygen was conducted by injecting certain volume of air via a syringe into the solution, which had been previously removed oxygen with pure nitrogen.

UV–Vis adsorption spectroscopies were carried out with a TU-1901 spectrophotometer. Scanning electron microscopy (SEM) was conducted with a S-3400 N at an acceleration voltage of 15 kV. Film samples for UV–Vis and SEM were fabricated respectively by using quartz slides, and the preparation process was similar to that of the films on the surface of GCE.

2.3 Preparation of modified electrode

Before modification, the bare glassy carbon disk electrodes (GCE, 3 mm in diameter) were polished to mirror-like with 1.0, 0.3, and 0.05 μm alumina slurry in metallographic sandpapers, then washed with double-distilled water and sonicated with double-distilled water for about 30 s.

The composite films were assembled on various solid substrates such as GCE and quartz slides. The experimental conditions for the assembly were optimized after a series of experiments.

The porous GO–CA films-modified GC electrode was fabricated by mixing SA with PEG as porogenic agent, and $CaCl_2$ as cross-linking agent. In general, four parts of PEG and one part of SA were added dropwise into about 20 mL 1 mg mL^{-1} GO sheets aqueous dispersion, followed by magnetic stirring for 2 h to form a homogenous suspension. While 10 μL of the mixture was dropped on the fresh prepared GCE surface, 5 μL of 0.1 g mL^{-1} $CaCl_2$ solution was sprayed over the mixture. A small bottle was fit over the electrode to serve as a closed evaporation chamber so that water evaporated slowly. The films were then dried and washed thoroughly using deionized water to ensure forming the porous GO–CA films-modified GC electrode.

For preparation of the porous Mb–GO–CA films on GC electrode surface, the same procedure was performed in the similar way described above. When 5 μL of 1 mg mL^{-1} Mb solution was cast onto the porous GO–CA films, a small bottle was fit tightly over the electrode so that water evaporated gradually. The porous Mb–GO–CA films were then dried in air overnight before measurement.

For comparison, ordinary GO–CA and ordinary Mb–GO–CA are fabricated through the same procedure but none PEG as a porogenic agent are used during the fabrication process.

3 Results and discussion

3.1 Characteristics of the porous GO–CA films

The morphologies of the porous GO–CA films and the porous Mb–GO–CA films were observed by SEM (Fig. 1). Compared with the porous CA films without GO sheets [40], the surface of porous GO–CA films (Fig. 1a) showed a rough porous structure and also displayed some flake-like structure, which may be attributed to the addition of GO sheets. After Mb was coated on the porous GO–CA films, the images appeared relatively smooth and featureless at the same magnification (Fig. 1b). These results indicated that Mb may have interacted with the porous GO–CA films, which changed the surface morphology of the porous

GO–CA films, and such composite films may be beneficial for proteins to retain its native structure.

3.2 Conformational studies

It was commonly known that the position of Soret absorption band of iron heme may provide information about possible denaturation of heme proteins [46]. To investigate the native structure of Mb, UV–Vis absorption of Mb immobilized in the porous Mb–GO–CA films was carried out. Both dry Mb films and the porous Mb–GO–CA films cast on the transparent quartz slides showed Soret band at 412 nm (Fig. 2a, b), indicating that Mb in the dry porous Mb–GO–CA films had the same secondary structure as the native state of Mb in dry Mb films alone. The dependence of the Soret band on pH of external solutions for the modified films was also tested. The results showed that the Soret band of Mb was sensitive to its microenvironment. At pH between 4.5 and 11.0, the Soret band appeared at 412 nm (Fig. 2c–g), suggesting that the Mb essentially retained its native state in the medium pH range. However, the Soret band showed peak shape distortion and was even hardly observed when pH was changed toward more acidic or basic direction (Fig. 2h, i), which demonstrated that Mb in porous Mb–GO–CA films might denature to considerable extent in this relatively extreme pH environment.

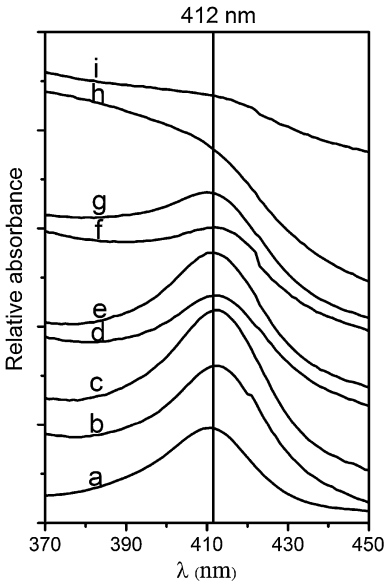

Fig. 2 UV–Vis spectra of Mb and the porous Mb–GO–CA films on quartz slides: (*a*) dry Mb film, (*b*) dry Mb–GO–CA film; and the porous Mb–GO–CA films in different pH buffer solutions: (*c*) pH 5.5, (*d*) pH 7.0, (*e*) pH 9.0, (*f*) pH 11.0, (*g*) pH 4.5, (*h*) pH 3.0, and (*i*) pH 12.0

3.3 Electrochemical impedance spectroscopy (EIS)

EIS is an effective method to get detailed information on the surface of modified electrodes. The impedance spectrum includes a semicircle part and a linear part, of which the semicircle part at higher frequencies corresponds to the electron-transfer-limited process and the linear part of lower frequencies corresponds to the diffusion process. And the diameter of the semicircle part is equal to the charge transfer resistance (R_{ct}) at the electrode surface [47]. Figure 3 displayed the impedance spectra in the form of Nyquist diagrams at different films with the redox probe of $[Fe(CN)_6]^{3-/4-}$ in a frequency range from 0.01 Hz to 100 kHz under its formal potential (0.17 V vs. SCE). The values of R_{ct} could be estimated by using the Randles equivalent circuit (the insert picture in Fig. 3) as the model and fitting the impedance data into the model [48]. For bare GCE, a small semicircle of Nyquist plot was observed (Fig. 3a) and the fitted R_{ct} was only 601.6 Ω. The fitted R_{ct} values for porous GO–CA, ordinary GO–CA, and porous CA films were 1,390.3, 2,133.0, and 3,512.5 Ω, respectively. Compared with ordinary GO–CA film, R_{ct} of porous GO–CA decreased more than 700 Ω, indicating that porous structure of the film may play an important role similarly to a conducting wire or electro-conducting tunnel, which may benefit the direct electron transfer between enzymes and

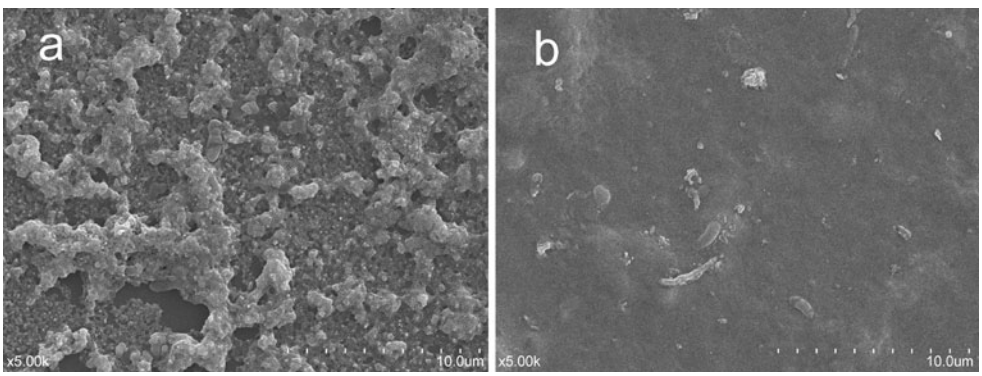

Fig. 1 SEM images of **a** the porous GO–CA films, **b** the porous Mb–GO–CA films

electrodes [49]. The effect of GO sheets on the electrochemical behavior of films was investigated by comparing R_{ct} of porous GO–CA with porous CA films, demonstrating that the GO–CA films assembled with GO had smaller R_{ct} than those with no GO sheets, which mainly attributed to the good conductivity of GO sheets.

While for the porous Mb–GO–CA films (Fig. 3e), the R_{ct} value was got as 4,596.5 Ω, which was much larger than the porous GO–CA. This may be attributed to the nonconductive properties of Mb which acted as an inert electron layer and hindered the electron transfer [50], demonstrating that Mb was immobilized successfully into the porous composite films on the electrode surface, and furthermore indicated that Mb immobilized in films may have an influence on the characterization of the porous GO–CA films.

3.4 Direct electrochemistry of Mb

The porous Mb–GO–CA films on GCE in protein-free pH 7.0 buffers gave pairs of well-defined, reversible CV peaks at −0.350 V versus SCE at the steady state after multiple scans (Fig. 4d). The peaks were located at the potentials characteristic of the heme Fe(III)/Fe(II) redox couples of the proteins [51]. No voltammetric peaks were observable for the porous GO–CA film-modified electrode in the same potential window (Fig. 4a). For the porous Mb–GO–CA films, the peak currents increased with soaking time and reached the steady state in about 0.5 h. Thus, all following electrochemical experiments were reported at the steady state after multiple scans.

The effect of scan rate on CVs of porous Mb–GO–CA film was studied. Both the anodic and cathodic peak currents were almost symmetrical and linearly proportional to

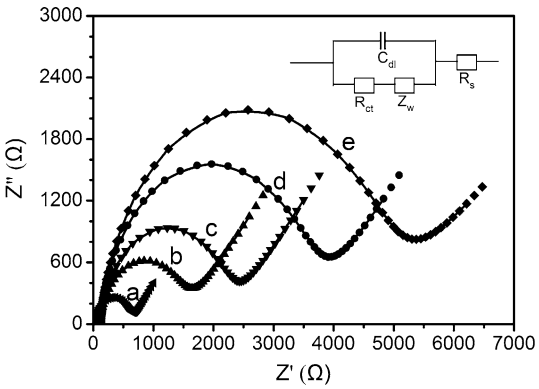

Fig. 3 Electrochemical impedance spectra for (*a*) bare GCE, (*b*) porous GO–CA film GC/GCE, (*c*) ordinary GO–CA/GCE, (*d*) porous CA/GCE, and (*e*) porous Mb–GO–CA/GCE in pH 7.0 buffers containing 5.0 mM $[Fe(CN)_6]^{3-/4-}$. The frequency range was from 0.01 to 100 kHz with perturbation amplitude of 5 mV. The *insert picture* in the top is the Randles equivalent circuit

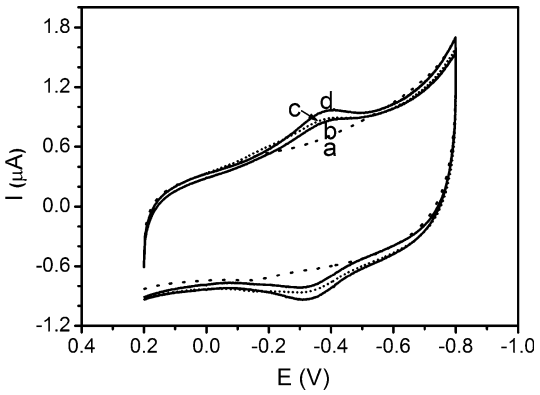

Fig. 4 Cyclic voltammograms of (*a*) porous GO–CA film, (*b*) porous Mb–CA film, (*c*) ordinary Mb–GO–CA film, and (*d*) porous Mb–GO–CA film in pH 7.0 buffers at a scan rate of 0.2 V s^{-1}

the scan rate and their potentials did not show considerable shift in the range from 0.1 to 2.0 V s^{-1}. Integration of reduction peak at these scan rates corresponded to nearly the same Q value. All these results demonstrated that the electrochemical behavior of Mb entrapped in the porous GO–CA film was a surface-controlled process [52]. According to the integration of the porous Mb–GO–CA film-modified electrodes at different scan rates and Faraday's law $Q = nFA\Gamma^*$ [53] (where n is the electron-transfer number, F is Faraday's constant, and A is the area of the electrode), the surface concentration (Γ^*) of electroactive Mb for the porous Mb–GO–CA film was estimated to be 1.65×10^{-11} mol cm^{-2}, which was larger than Γ^* of electroactive Mb for the ordinary Mb–GO–CA film (Table 1). It was possible that the porous GO–CA film provided a larger surface area for protein binding and enhanced the loading of Mb protein molecules.

For comparison, the direct electron transfer of the porous Mb–CA film without GO sheets and the ordinary Mb–GO–CA films on electrodes were investigated by CV method (Table 1). It was obvious that the anodic and cathodic peak currents (I_{pc}) of Mb at the porous Mb–GO–CA films was higher than that at the ordinary Mb–GO–CA films or the porous Mb–CA films-modified electrodes (Fig. 4b or c). And the porous Mb–GO–CA films exhibited much better symmetric oxidation and reduction peaks, where the separation (ΔE_p) between the anodic and the cathodic peak potential was the smallest among the three films. This order of sequence was in good agreement with that of the porosity or permeability for the films demonstrated in the EIS experiment.

3.5 Square-wave voltammetry (SWV)

SWV is easier to analyze theoretically and treat quantitatively, and also has the advantage in signal–noise ratio and resolution over CV [54]. SWV was used here to estimate

Table 1 The electrochemical parameters for different Mb-films on GCE

Films	CV				SWV	
	$E^{o\prime}$ (V vs. SCE)	ΔE_p (mV)	I_{pc} (μA)	Γ^* (mol cm^{-2})	$E^{o\prime}$(V vs. SCE)	k_s (s^{-1})
Porous Mb–CA[43]	−0.340	66	1.736	9.18×10^{-11}	−0.339	28.18
Ordinary Mb–GO–CA	−0.348	49	0.1380	1.12×10^{-11}	−0.326	35.98
Porous Mb–GO–CA	−0.350	45	0.2033	1.65×10^{-11}	−0.329	36.29

$E^{o\prime}$ the formal potential estimated as average of reduction and oxidation peak potentials, $\Delta E_p = E_{pa} - E_{pc}$ the separation between the anodic and the cathodic peak potentials, I_{pc} the cathodic peak current, Γ^* the surface concentration of electroactive Mb in different modified films. These data were estimated by CVs in pH 7.0 buffers

the average apparent heterogeneous electron transfer rate constant (k_s) and formal potential ($E^{o\prime}$) with nonlinear regression analysis. The fitting model for SWV forward and reverse curves was a combination of thin-layer SWV model and the $E^{o\prime}$ dispersion model, which was described in detail in previous literatures [55, 56].

The analysis of SWV data for porous Mb–-GO–CA films showed goodness of fits on the 5-$E^{o\prime}$ dispersion model over a range of amplitudes and frequencies (Fig. 5). The value of k_s obtained from fitting SWV data at pH 7.0 was 36.29 s^{-1} and the average $E^{o\prime}$ was −0.329 V versus SCE (Table 1). The k_s and $E^{o\prime}$ values for other Mb film systems obtained by the same method are listed in Table 1 for comparison. The k_s value of Mb–GO–CA films is in the same order as that of other Mb films [43] and relatively large, qualitatively in agreement with the quasi-reversible CV behavior of the films. The $E^{o\prime}$ value obtained by SWV for Mb–GO–CA films was in close to that estimated by CV, but different from that for Mb in other types of films, which confirms a specific influence of film environment on $E^{o\prime}$ of heme proteins as reported previously [55, 57]. Film components may change potentials via interactions with the protein or by their influence on the electrode double layer [28].

A comparison was made to show the advantages of the porous Mb–GO–CA films modified on the electrode surface as shown in Table 1. It can be seen that the cathodic peak current (I_{pc}) of the porous Mb–GO–CA films was the largest among the three films. Besides, the separation (ΔE_p) between the anodic and cathodic peak potentials of the porous Mb–GO–CA films was smaller than that of the ordinary Mb–GO–CA films, as well as the porous Mb–GO films. The analysis of SWV data for the porous Mb–GO–CA films showed that the value of k_s was larger than those of other similar protein films, such as 35.98 s^{-1} for the ordinary Mb–GO–CA film, 28.18 s^{-1} for the porous Mb–CA films (Table 1), and 25.05 s^{-1} for Mb–GO-Nafion film [45]. It thus can be concluded that the porous Mb–GO–CA films displayed the best performance on enhancing the electron transfer between Mb and the electrodes, and these results proved the effect of GO sheets on the

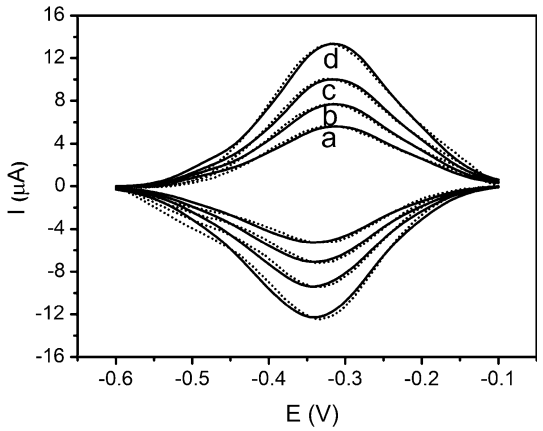

Fig. 5 Square-wave forward and reverse current voltammograms for porous Mb–GO–CA films in pH 7.0 buffers at different frequencies. *Dashed lines* represent the experimental SWV from which the background has been subtracted. *Solid lines* are the best fit obtained by nonlinear regression onto the 5-$E^{o\prime}$ dispersion model. SWV condition: pulse height: 60 mV, step height 4 mV, and frequencies (Hz): (*a*) 140; (*b*) 160; (*c*) 180; (*d*) 200

electrochemical behavior of Mb in the porous GO–CA films, demonstrating that the porous Mb–GO–CA films assembled with GO had a much high-electron transfer rate, higher maximum surface concentration of electroactive Mb than those with no GO sheets, which could be attributed to the addition of GO sheets as well as porous structure of the composite films on providing a more favorable microenvironment for Mb and play an important role in facilitating the direct electron exchange between the electrode and the active center of enzyme.

3.6 Electrocatalytic reactivity

Farmer and co-workers [58] studied electrocatalytic reduction of NO_2^- with the Mb–DDAB films on PG electrodes, and they found that under acidic conditions, the NO_2^- species underwent a disproportionation reaction. Electrochemical catalytic reduction of nitrite was tested with the porous Mb–GO–CA films. When NO_2^- was added into a pH 5.0 buffer, a new reduction peak was observed at about −0.75 V (Fig. 6d, e) while the original

MbFe(III)/Fe(II) peak pair remained intact (Fig. 6c). Direct reduction of NO_2^- at porous GO–CA films without Mb was found at the potential more negative than −1.1 V (Fig. 6b). Thus porous Mb–GO–CA films lowered the reduction overpotential for NO_2^- by shift 0.35 V. The catalytic reduction current increased linearly with the concentration of NO_2^- in the range of 1.0–6.0 mM with a detection limit of 0.25 mM and a correlation coefficient of 0.998. When the concentration of NO_2^- was higher than 7.0 mM, a response platform emerged in the catalytic peak current, showing typical Michaelis–Menten kinetic characteristic of protein-based electrodes. The apparent Michaelis–Menten constant (K_M^{app}) provides an indication of the enzyme-substrate kinetics and it can be estimated from Lineweaver–Burk equation [59]:

$$1/I_{ss} = (K_M^{app}/I_{max}C) + (1/I_{max})$$

here I_{ss} is the steady-state current after the addition of substrate, C is the bulk concentration of the substrate, and I_{max} is the maximum current measured under saturated substrate conditions. The value of K_M^{app} can be obtained by the analysis of slope and intercept from the plot of I_{ss}^{-1} versus C^{-1}. The K_M^{app} was calculated to be 1.82 mM, which was smaller than Mb on the SA–Mb–IL–Fe_2O_3/CILE [60] and GNRs@SiO_2/RTIL-sol–gel/GCE [61]. This indicated that Mb immobilized in porous GO–CA film retained its bioactivity and maintains a high-biological affinity to NO_2^-.

Catalytic reduction of oxygen by the porous Mb–GO–CA films was further examined by CV. When a certain amount of air was passed through a pH 7.0 buffer solution by a syringe, a significant increase in the reduction peak at about −0.37 V was observed. This was accompanied by a decrease and disappearance of the MbFe(II) oxidation peak (Fig. 7A d, e). The reduction peak current for MbFe(III) increased as the concentration of air increased. Catalytic efficiency was expressed as the ratio of the reduction peak current of MbFe(III) in the presence (I_c) and in the absence (I_d) of oxygen, I_c/I_d. The value of I_c/I_d decreased with an increase in the scan rate (Fig. 7B). All these results are characteristic of oxygen by electrochemical catalysis with Mb in [62].

For electrocatalytic reduction of H_2O_2, a typical catalytic reduction peak at the porous Mb–GO–CA was shown in Fig. 8A, which was very similar to the behavior of O_2. When H_2O_2 was added into the electrochemical cell, a dramatically increase of reduction peak at about −0.39 V was observed and accompanied by the decrease of the oxidation peak, indicating a typical electrocatalytic reduction process of H_2O_2. No reduction peak of H_2O_2 was obtained in the presence (Fig. 8A b) or in the absence (Fig. 8A a) of H_2O_2 for porous GO–CA films, indicating that the reduction of H_2O_2 was catalyzed by Mb entrapped

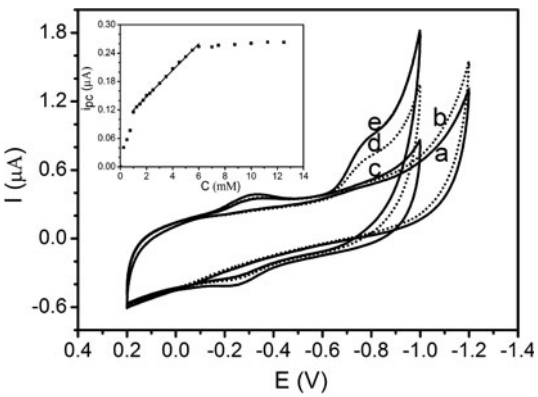

Fig. 6 Cyclic voltammograms at a scan rate of 0.1 V s^{-1} in 8 mL of pH 5.0 buffers for porous GO–CA films with (*a*) no $NaNO_2$, (*b*) 2.5 mM $NaNO_2$, and for porous Mb–GO–CA films with (*c*) no $NaNO_2$, (*d*) 2.5 mM $NaNO_2$, (*e*) 5.0 mM $NaNO_2$. *Inset* the calibration curve of reduction peak currents and concentrations of $NaNO_2$

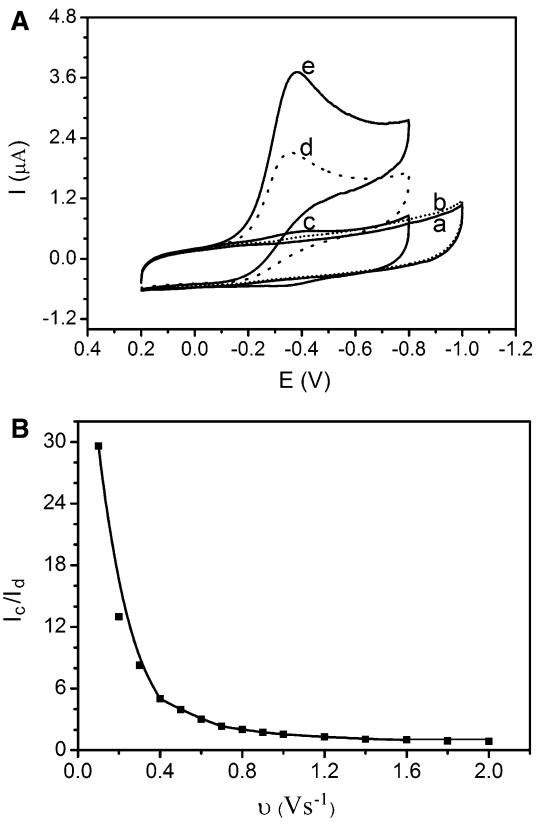

Fig. 7 **a** Cyclic voltammograms at a scan rate of 0.1 V s^{-1} in 8 mL of pH 7.0 buffers for porous GO–CA films with (*a*) no O_2 present, (*b*) 20 mL of air was injected into the sealed cell, and for porous Mb–GO–CA films with (*c*) no O_2 present, (*d*) 20 mL, and (*e*) 40 mL of air was injected respectively. **b** Influence of scan rate on catalytic efficiency (I_c/I_d) in pH 7.0 buffers, for porous Mb–GO–CA films in 8 mL pH 7.0 buffers, where I_d is the CV reduction peak current without oxygen and I_c is the CV reduction peak current with 10 mL of air injected

in porous GO–CA films. The possible electrode reaction between Mb and H_2O_2 could be expressed as follows [63]:

$$\mathrm{MbFe(III)} + \mathrm{H_2O_2} \rightarrow \mathrm{Compound\ I} + \mathrm{H_2O} \quad (1)$$

$$\mathrm{Compound\ I} + \mathrm{H_2O_2} \rightarrow \mathrm{MbFe(III)} + \mathrm{O_2} \quad (2)$$

$$\mathrm{MbFe(III)} + \mathrm{e^-} \rightarrow \mathrm{MbFe(II)} \quad \text{at electrode} \quad (3)$$

$$\mathrm{MbFe(II)} + \mathrm{O_2} \rightarrow \mathrm{MbFe(II)} - \mathrm{O_2} \quad \text{fast} \quad (4)$$

$$\mathrm{MbFe(II)} - \mathrm{O_2} + 2\mathrm{e^-} + 2\mathrm{H^+} \rightarrow \mathrm{MbFe(II)} + \mathrm{H_2O_2} \quad \text{at electrode} \quad (5)$$

From above process MbFe(III) was efficiently converted to its reduced form, MbFe(II), in the presence of H_2O_2. Thus, the reduction current increased after the addition of H_2O_2. The reduction peak current versus concentration of H_2O_2 was plotted, and a linear relationship in a range from 2.5 to 56.25 μM with the linear regression coefficient of 0.999 was obtained and the detection limit was 1.25 μM. Based on this linear response of reduction current with H_2O_2 concentration, H_2O_2 could be detected quantitatively.

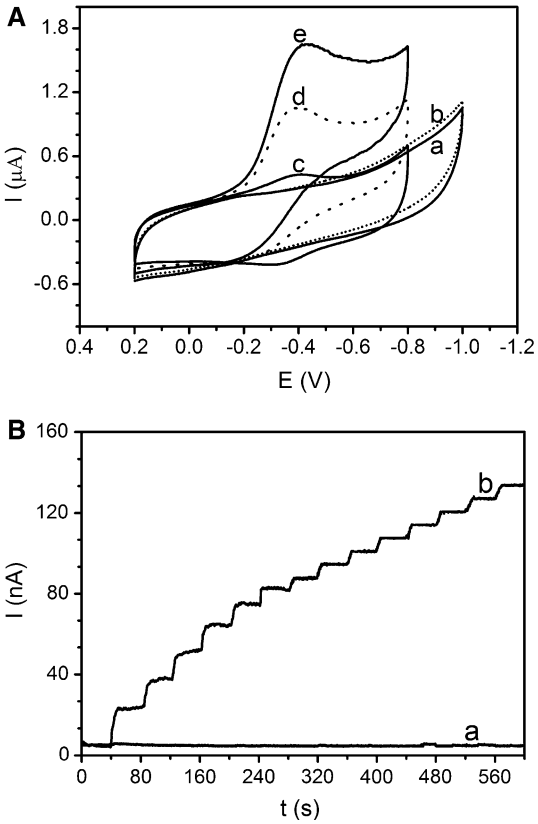

Fig. 8 **a** Cyclic voltammograms at 0.1 V s^{-1} in 8 mL of pH 7.0 buffers for porous GO–CA films with (*a*) no H_2O_2, (*b*) 18.75 μM H_2O_2, and for porous Mb–GO–CA films with (*c*) no H_2O_2, (*d*) 18.75 μM H_2O_2, (*e*) 37.5 μM H_2O_2. **b** Amperometric response of (*a*) porous GO–CA film and (*b*) porous Mb–GO–CA film at −0.17 V in pH 7.0 buffers solution with 6.25 μM H_2O_2 injected every 40 s

The porous Mb–GO–CA modified electrode also revealed good amperometric responses for electrocatalytic reduction of H_2O_2. Upon the successive addition of H_2O_2 to the buffer solution, the reduction current increased rapidly to reach a stable value in less than 6 s (Fig. 8B). The fast response could be attributed to the fast diffusion process on electrode surface and the high-electronic conductivity of porous GO–CA composite film.

Catalytic efficiencies and detection limit for different substrates ($NaNO_2$, O_2, and H_2O_2) with the porous Mb–CA, Mb–GO–CA, and Mb–GO-Nafion [45] films were listed in Table 2 for comparison.

Compared with the porous Mb–CA films [43] and Mb–GO-Nafion [45], the porous Mb–GO–CA films showed higher catalytic efficiency toward reduction of O_2 and H_2O_2, and could detect a lower concentration of NO_2^- (as shown in Table 2). These could be attributed to the good conductivity and the high biocompatibility of GO sheets, and the large specific surface area of the porous structure of the composite films, which made the adsorbed Mb in the films retain its near native structure and showed excellent biocatalytic activity.

3.7 Stability and reproducibility

Stability is an important parameter to evaluate the performance of a biosensor. The stability of the porous Mb–GO–CA films was tested by CV with the following methods. First, the 30 continuous cyclic scans were carried out at a scan rate of 0.2 V s^{-1}. No obvious decrease of the voltammetric response was observed. Simultaneously, the long-term storage stability of the porous Mb–GO–CA films was also investigated. The sensor was stored in buffers in a refrigerator at 4 °C when not being in use. The electrochemical response to 6.25 μM H_2O_2 in the pH 7 buffers was determined. A slightly decrease of the current response was observed during the first 7 days (90 % remained), and the catalytic current response to H_2O_2 almost remained unchanged after 2 weeks, and

Table 2 Catalytic efficiency or detection limit of different substrates with different films

Films	Substrates		
	Catalytic efficiency (I_c/I_d)		Detection limit (mM)
	O_2 [a]	H_2O_2 [b]	NO_2^-
Mb–CA[43]	1.451	1.346	1.25
Mb–GO–CA	10.68	3.205	0.25
Mb–GO–Nafion[45]	1.8195	1.214	0.75

[a] 20 ml of air was passed in 8 ml of solution at 0.2 V s^{-1}

[b] 12.5 μM of H_2O_2 was injected in 8 ml of solution at 0.1 V s^{-1}

could retain 84 % of its initial activity to H_2O_2 after 30 days. These results suggested that the modified electrode exhibited a good operational stability for the electrochemical detection of H_2O_2. It can be attributed to the mild enzyme immobilization condition and the composite protective layer. Besides, the GO sheets with good biocompatibility can provide favorable architecture for retaining the enzyme bioactivity.

In addition, four modified electrodes were prepared by the same procedure independently and the relative standard deviation (RSD) for the determination of 10 μM H_2O_2 by CV measurements was calculated as 2.59 % (from measurement of anodic peak currents), indicating that the porous Mb–GO–CA films modified electrode has good reproducibility in both the preparation procedure and the voltammetric determinations.

4 Conclusions

In conclusion, GO sheets can be incorporated in the porous CA films and used to immobilize Mb to construct a more efficient biosensor. Mb entrapped in the as-prepared porous Mb–GO–CA films retained its native state and gave a direct, reversible electron transfer with underlying electrodes. The immobilized GO sheets dramatically enhanced the performance of Mb on the porous GO–CA composite film electrodes, which has been demonstrated by EIS and voltammetry results. The excellent performance is mainly attributed to the good conductivity, the high biocompatibility of GO sheets, and the large specific surface area of the porous structure of the composite films. The porous GO–CA films provide a more favorable microenvironment for Mb and play an important role in promoting the direct electron exchange between the electrode and the active center of enzyme. Mb act as an enzyme-like catalyst in the porous Mb–GO–CA films on electrodes exhibited good electrocatalytic response toward various substrates, such as $NaNO_2$, O_2 and H_2O_2, and displayed an excellent sensing performance with high sensitivity and good stability, which demonstrate the potential applications in fabrication of novel biosensor or bioreactors.

Acknowledgments This work was supported by the National Natural Science Foundation of China (Grant No. 21175059), the Taishan Scholars Program of Shandong Province, and the Growing Base for State key Laboratory of Qingdao University.

References

1. Eda G, Fanchini G, Chhowalla M (2008) Nat Nanotechnol 3:270–274
2. Geim AK, Novoselov KS (2007) Nature Mater 6:183–191
3. Lee C, Wei X, Kysar JW, Hone J (2008) Science 321:385–388
4. Martin N, Sanchez L, Illescas B, Perez I (1998) Chem Rev 98:2527–2547
5. Shan CS, Yang HF, Song JF, Han DX, Ivaska A, Niu L (2009) Anal Chem 81:2378–2382
6. He YP, Sheng QL, Zheng JB, Wang MZ, Liu B (2011) Electrochim Acta 56:2471–2476
7. Leenaerts O, Partoens B, Peeters FM (2008) Phys Rev B 77:125416
8. Ang PK, Chen W, Wee ATS, Loh KP (2008) J Am Chem Soc 130:14392–14393
9. Xu HF, Dai H, Chen GN (2010) Talanta 81:334–338
10. Wang Y, Li Y, Tang L, Lu J, Li J (2009) Electrochem Commun 11:889–892
11. Shan CS, Yang HF, Han DX, Zhang QX, Ivaska A, Niu L (2010) Biosens Bioelectron 25:1504–1508
12. Li J, Guo SJ, Zhai YM, Wang EK (2009) Anal Chim Acta 649:196–201
13. Shan CS, Yang HF, Han DX, Zhang QX, Ivaska A, Niu L (2010) Biosens Bioelectron 25:1070–1074
14. Kang X, Wang J, Wu H, Aksay IA, Liu J, Lin Y (2009) Biosens Bioelectron 25:901–905
15. Yang S, Guo D, Su L, Yu P, Li D, Ye J, Mao L (2009) Electrochem Commun 11:1912–1915
16. Casero E, Alonso C, Văzquez L, Petit-Domĭnguez MD, Parra-Alfambra AM, de la Fuente M, Merino P, Ălvarez-Garcĭa S, de Andrĕs A, Pariente F, Lorenzo E (2013) Electroanalysis 25(1):154–165
17. Schniepp HC, Li JL, McAllister MJ, Sai H, Herrera-Alonso M, Adamson DH, Prud'homme RK, Car R, Saville DA, Aksay IA (2006) J Phys Chem B 110:8535–8539
18. Bai H, Li C, Wang X, Shi G (2010) Chem Commun 46:2376–2378
19. Wu SX, Yin ZY, He QY, Huang X, Zhou XZ, Zhang H (2010) J Phys Chem C 114:11816–11821
20. Zhang LL, Zhou R, Zhao XS (2010) J Mater Chem 20:5983–5992
21. Zhang JL, Zhang F, Yang HJ, Huang XL, Liu H, Zhang JY, Guo SW (2010) Langmuir 26:6083–6085
22. Zhou M, Zhai Y, Dong S (2009) Anal Chem 81:5603–5613
23. Wu H, Wang J, Kang X, Wang C, Wang D, Liu J, Aksay IA, Lin Y (2009) Talanta 80:403–409
24. Zuo XL, He SJ, Li D, Peng C, Huang Q, Song SP, Fan CH (2010) Langmuir 26:1936–1939
25. Stryer L (1988) Biochemistry, 3rd edn. WH Freeman, New York
26. Armstrong FA, Hill HAO, Walton NJ (1988) Acc Chem Res 21:407–413
27. Santucci R, Campanella L (1994) Curr Top Electrochem 3:313–328
28. Rusling JF (1998) Acc Chem Res 31:363–369
29. Walt DR (1988) Acc Chem Res 31:267–278
30. Zhou Y, Yang H, Chen HY (2008) Talanta 76:419–423
31. Nassar AEF, Bobbitt JM, Struart JD, Rusling JF (1995) J Am Chem Soc 117:10986–10993
32. Sun H, Hu NF, Ma HY (2000) Electroanalysis 12:1064–1070
33. Zhang L, Zhang Q, Li JH (2007) Electrochem Commun 9:1530–1535
34. Zhan T, Xi M, Wang Y, Sun W, Hou W (2010) J Colloid Interface Sci 346:188–193
35. Ding C, Zhang M, Zhao F, Zhang S (2008) Anal Biochem 378:32–37
36. Shinohara M, Nishida R, Aoyama T, Kamono H, Bando H, Nishizawa M (2000) Fish Sci 66:616–617
37. Braccini I, Pérez S (2001) Biomacromolecules 2:1089–1096
38. Jen AC, Wake MC, Mikos AG (1996) Biotechnol Bioeng 50:357–364
39. Zhao H, Zheng W, Meng Z, Zhou H, Xu X, Li Z, Zheng Y (2009) Biosens Bioelectron 24:2352–2357

40. Sun W, Wang D, Gao R, Jiao K (2007) Electrochem Commun 9:1159–1164
41. Wu L, Ding J (2004) Biomaterials 25:5821–5830
42. Ko HF, Sfeir C, Kumta PN (2007) Mater Sci Eng C 27:479–483
43. Li Q, Sun H, Liu X, Zhao XS (2012) J Solid State Electrochem 16:1651–1661
44. Hummers WS, Offeman RE (1958) J Am Chem Soc 80:1339
45. Guo C, Sun H, Zhao XS (2012) Sens Actuators B 164:82–89
46. George P, Hanania G (1953) Biochem J 55:236–243
47. Wang M, Sheng Q, Zhang D, He Y, Zheng J (2012) Bioelectrochemistry 86:46–53
48. Bard AJ, Faulkner LR (2001) Electrochemical methods: fundamentals and applications, 2nd edn. Wiley, New York
49. Zhao J, Henkens RW, Stonehuerner J, O'Daly JP, Crumbliss AL (1992) J Electroanal Chem 327:109–119
50. Fei W, Zhang Y, Sun X, Zhang Y, Cao H, Shen H, Jia N (2012) J Electroanal Chem 675:5–10
51. Zhao GC, Zhang L, Wei XW, Yang ZS (2003) Electrochem Commun 5:825–829
52. Li Y, Li Y, Yang Y (2011) Bioelectrochemistry 8:112–116
53. Murray RW, Bard AJ (eds) (1984) Electroanalytical chemistry. Marcel Dekker, New York
54. Osteryoung JG, O'Dea JJ, Bard AJ (eds) (1986) Electroanalytical chemistry. Marcel Dekker, New York
55. Nassar AEF, Zhang Z, Hu NF, Rusling JF, Kumosinski TF (1997) J Phys Chem 101:2224–2231
56. Zhang Z, Rusling JF (1997) Biophys Chem 63:133–146
57. Hu NF, Rusling JF (1997) Langmuir 13:4119–4125
58. Lin R, Bayachou M, Greaves J, Farmer PJ (1997) J Am Chem Soc 119:12689–12690
59. Kamin RA, Wilson GS (1980) Anal Chem 52:1198–1205
60. Zhan T, Xi M, Wang Y, Sun W, Hou W (2010) J Colloid Interface Sci 346:188–193
61. Zhu WL, Zhou Y, Zhang JR (2009) Talanta 80:224–230
62. Andrieux CP, Blocman C, Dumas-Bouchiant JM, Saveant JM (1979) J Am Chem Soc 101:3431–3441
63. Huang R, Hu NF (2001) Bioelectrochemistry 54:75–81